

RESEARCH

Open Access



Study on the resistance coefficient of hot dry rock cuttings in Herschel-Bulkley fluid: experiments and modeling

Lei Wang^{1,3}, Jinhui Li^{2*} , Jianjun Zhao^{1,3}, Shuolong Wang¹ and Zheng Chu¹

*Correspondence:
18813156602@163.com

¹ Sinopec Research Institute of Petroleum Engineering, Co., Ltd, Beijing 102206, China

² School of Petroleum Engineering, Northeast Petroleum University, Daqing 163318, China

³ Key Laboratory of Geothermal Resources Exploitation and Utilization, SINOPEC, Beijing 100083, China

Abstract

Most hot dry rock geothermal wells are small angle directional wells, and rock cuttings easily accumulate at the bottom of the borehole to form a cuttings bed, causing accidents such as drill sticking, reducing the rate of penetration, and drilling tool breakage. Accurately calculating the resistance coefficient and settling velocity of hot dry rock cuttings can improve cuttings transportation efficiency, design and optimize drilling hydraulic parameters, and is crucial to solving borehole cleaning problems. Through visual experiments, this paper obtained experimental data on the settlement of 167 groups of spherical pellets, 153 groups of granite cuttings, and 174 groups of carbonate cuttings in the Herschel-Bulkley fluid. First, a prediction model for the resistance coefficient of spherical pellets consistent with Herschel-Bulkley fluid was established. Based on this, form factor-Roundness is introduced as the starting point, and two prediction models for the resistance coefficients of granite cuttings and carbonate cuttings in the Herschel-Bulkley fluid were established. The average relative errors between the resistance coefficient model predictions and experimental measurements are 9.61% for granite cuttings and 6.59% for carbonate cuttings. The average relative errors between the predicted and measured values of settlement velocity are 7.27% for granite cuttings and 6.21% for carbonate cuttings, respectively, which verifies the accuracy and reliability of the prediction model. The research results can provide a theoretical basis and engineering application guidance for optimizing drilling fluid rheology and circulation displacement in engineering.

Keywords: Borehole cleaning, Dry hot rock geothermal well, Cuttings settlement, Resistance coefficient, Herschel-Bulkley fluid

Introduction

China's geothermal resources are widely distributed and have large reserves [1]. Songliao Basin, Hepu Basin, Gonghe Basin, and Subei Basin are all important areas for geothermal resource exploitation [2–5]. At present, most of the dry hot rock geothermal wells that have been developed are small angle directional wells (the maximum well deviation angle is less than 30°). Compared with vertical wells, cuttings produced during drilling are more likely to accumulate at the bottom of the borehole under the influence of gravity, and the temperature of the hot dry rock is usually higher than 200 °C. High

temperature causes the viscosity of the drilling fluid to decrease, and the cutting-carrying ability is reduced, so cuttings will accumulate for a long time to form a cuttings bed. The formation of cutting beds will shorten the life of drilling tools, increase the risk of drill stuck, reduce drilling efficiency, and increase drilling costs. Therefore, the poor borehole cleaning effect is a problem that must be solved when drilling dry hot rock geothermal wells.

Researchers have conducted a large number of experimental studies on the settlement laws of spherical pellets in Newtonian and non-Newtonian fluids (mainly power law fluids) and established different forms of prediction models for settlement resistance coefficients. However, hot dry rock cuttings have different shapes and are highly irregular, and the rheology of the drilling fluid is more consistent with the Herschel-Bulkley fluid or Bingham fluid [6]. There are not many studies using the Herschel-Bulkley rheological model to model the sedimentation resistance coefficient. Among them, the Herschel-Bulkley rheological model was used in the research of Ahonguio, Elgaddafi, Hakim et al. However, their study focused on settling velocity rather than drag coefficient, and the experiments did not use real rock cuttings [7–9]. The experiments in this paper used real granite cuttings and carbonate cuttings. Moreover, during the drilling process of hot dry rock wells and deep wells, researchers try to add polyethylene beads, nanosilica nanoparticles, and other substances to the drilling fluid to improve the high-temperature resistance of the drilling fluid. The addition of these substances will make the rheological model of the drilling fluid closer to the Herschel-Bulkley fluid [10–14]. Therefore, directly using previous prediction models may produce large errors. To maximize accuracy, this paper first established a prediction model for the settlement resistance coefficient of spherical pellets in Herschel-Bulkley fluid through experiments. Using the form factor-roundness as the “bridge”, models for predicting the resistance coefficients of granite cuttings and carbonate cuttings in Herschel-Bulkley fluid were established. Based on two resistance coefficient prediction models, the settling velocities of the cuttings were derived by iteration, and the accuracy of the two dry-heat rock cuttings models was verified based on the average relative error between the calculated settling velocity prediction and the experimental settling velocity measurements. The particle settling resistance coefficient is a link in the study of solid–liquid phase interactions, and it is necessary to use the resistance coefficient to calculate the solid–liquid phase drag force in the modeling of cuttings transport. Therefore, the study of the settling resistance coefficient of dry hot rock cuttings in the Herschel-Bulkley fluid can help calculate the height of the cuttings bed, provide theoretical support for adjusting the viscosity of the drilling fluid and the mud pump discharge to obtain the maximum hydraulic energy distribution at the bottom of the well, and help to solve the borehole cleaning problem.

Experimental equipment and materials

Experimental equipment

The settlement experiment was conducted in a plexiglass cylinder with a height of 1500 mm and an inner diameter of 100 mm. Using a high-speed camera to record the movement of spheres and cutting pellets, The high-speed camera is a Revealer 2F04C, which achieves a frame rate of 190 FPS in full frame resolution (2320 × 1720) and 1260 FPS in 640 × 480 format, with intelligent image triggering, support for post-triggering,

and support for simultaneous shooting by several cameras. the computer stores and analyzes experimental data. The observation area of the high-speed camera is located between 750 mm from the top of the column and 350 mm from the bottom of the column, ensuring that the pellets can be balanced by forces above the observation area to reach the final settling velocity while avoiding the influence of the end effect.

When pellets settle, they will be subject to forces from the solution in all directions, so rotation and displacement will occur during the sinking process. To determine whether the pellets have reached a stable settlement state, the observation area was divided into several small segments during the experiment, and the settling velocity of the pellets was compared with that of each small segment. If the velocity of the pellets in each segment was the same or the difference was less than 5%, it was considered that the pellets had achieved stable settlement.

Experimental particle and dry heat rock cuttings shape description

Precision solid spherical pellets made of iron, zirconia, silicon nitride, and aluminum were used in this experiment. Although the cuttings produced during actual oil and gas drilling construction have a much lower density and settling rate than spherical pellets of the same mass, the use of some high-density materials can increase the applicability of the data. The physical properties of the pellets used in the experiment are shown in Table 1, and the granite cuttings and carbonate cuttings used are shown in Fig. 1.

It can be seen that granite cuttings are mostly flaky, while carbonate cuttings are predominantly massive. To better characterize the shape of irregular pellets, researchers have proposed more than a dozen different form factors. Considering the

Table 1 Physical properties of pellets used in experiments

Materials	Equivalent diameter D_e (mm)	Density (kg/m ³)
Iron	1, 2, 3, 4, 5	7850
Zirconia	1, 2, 3, 4, 5	6040
Silicon nitride	1.5, 2, 3, 4, 5	3250
Aluminum	1, 2, 3, 4, 5, 6	2700
Granite cuttings	1.6–5.1	2810
Carbonate cuttings	2.3–4.6	2440



Fig. 1 Two types of hot dry rock cuttings

accuracy of experimental studies and the convenience of practical engineering, this paper adopts the roundness proposed by Wadell *H* (1932) to describe the highly irregularly shaped rock chip pellets [15, 16]. Roundness is defined as shown in Eq. (1):

$$X = \frac{P_a}{P_b} \tag{1}$$

where.

P_a : perimeter of the equivalent sphere of the projected surface of the particle, m ,

P_b : the projected perimeter of the particle, m .

The roundness of the cuttings can be measured using the “analyze pellets” function in the image analysis software ImageJ, ImageJ is a scientific image analysis tool that can scale, rotate, and blur images, as well as analyze a range of geometric features of an object within a selected area, including length, angle, perimeter, area, circularity, and more. the measurement conversion diagram is shown in Fig. 2.

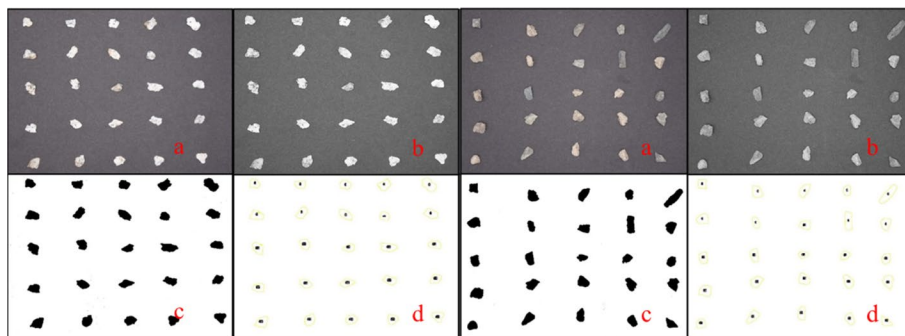
The experiment obtained 327 sets of valid dry heat rock cuttings settlement data, including 153 sets of granite cuttings and 174 sets of carbonate cuttings. Statistics and analyses of the roundness and equivalent diameter D_e of the two types of cuttings show that the equivalent diameter of the granite cuttings D_{eg} used for the experiment ranges from 1.6 to 5.1 mm, and the Roundness ranges from 0.297 to 0.813, while the equivalent diameter of the carbonate cuttings D_{ec} used for the experiment ranges from 2.3 to 4.6 mm, and the Roundness ranges from 0.457 to 0.863. The results are shown in Fig. 3. It can be seen that the Roundness of both dry heat rock cuttings is less than that of spherical pellets. The particle equivalent diameter is defined as shown in Eq. (2):

$$D_e = \left(\frac{6m_p}{\pi\rho_s} \right)^{\frac{1}{3}} \tag{2}$$

where.

m_p : quality of pellets, kg,

ρ_s : density of pellets, kg/m^3 .



Granite cuttings: a. original image; b. grayscale image Carbonate cuttings: a. original image; b. grayscale image

; c. threshold image; d. silhouette image ; c. threshold image; d. silhouette image

Fig. 2 Conversion diagram of two types of dry hot rock cuttings. Granite cuttings: **a** original image, **b** grayscale image, **c** threshold image, **d** silhouette image. Carbonate cuttings: **a** original image, **b** grayscale image, **c** threshold image, **d** silhouette image

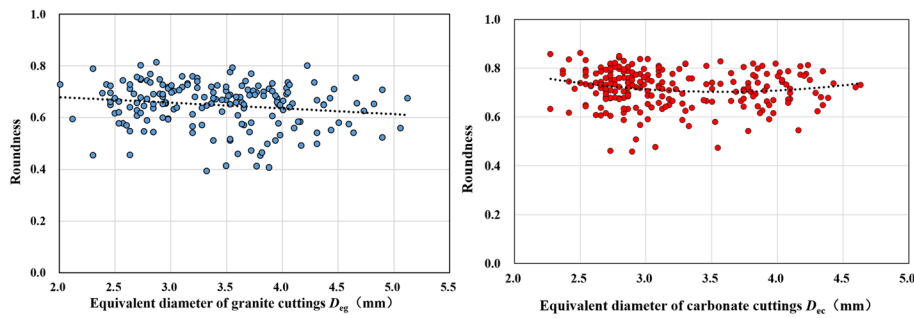


Fig. 3 Relationship between Roundness and equivalent diameter of two types of dry hot rock cuttings

Experimental solution and rheological parameter testing

In this experiment, Carbomer 980 powder was mixed with water to prepare the test solution. Carbomer 980 is a polyacrylic acid cross-linked polymer with acid groups in the molecular chain, which needs to be neutralized by adding Trolamine solution (content $\geq 99.0\%$ (GC)), After neutralization, carbomer solution forms a clear gel. Most importantly, the rheological model of the carbomer solution is consistent with the Herschel-Bulkley fluid as shown in Eq. (3):

$$\tau = \tau_0 + K\dot{\gamma}^n \tag{3}$$

where.

- τ : shear stress, Pa;
- τ_0 : yield point, Pa;
- $\dot{\gamma}$: shear rate, 1/s.

A small amount of carbomer solution was taken before the start of the settlement experiments and its rheological profile at the current experimental temperature was measured using an Anton Paar MCR 92 rheometer, and fitted using data analysis software. The Herschel-Bulkley fluid rheological model was used to fit 6 groups of carbomer solutions with different concentrations. The average value of the coefficient of determination R^2 after fitting was as high as 0.9917, proving that the rheological model of the carbomer solution is consistent with the Herschel-Bulkley fluid. To make the rheology of the prepared carbomer solution closer to that of the actual drilling fluid at the drilling site, the consistency coefficient K needs to be in the range of 0.01–0.05 Pa.sⁿ, and the test results are as shown in Table 2.

Table 2 Rheological test results of Carbopol aqueous solution for experiment

Test solution	Mass concentration (wt%)	T (°C)	Solution density (kg/m ³)	Parameters			R ²
				τ_0 (Pa)	K (Pa.s ⁿ)	n	
Carbomer solution	0.075	25.01	1000	0.289	0.0498	0.829	0.9958
	0.07	24.89	1000	0.254	0.0382	0.859	0.9949
	0.065	24.99	1000	0.231	0.0266	0.903	0.9934
	0.06	25.04	1000	0.206	0.0176	0.949	0.9899
	0.055	25.03	1000	0.192	0.0145	0.965	0.9936
	0.05	24.97	1000	0.110	0.0119	0.981	0.9825

Equations (4)–(6) are common drilling fluid rheology formulas. Table 3 is a comparison of the rheological properties of the carbomer solution calculated by equations and the rheological properties of the carbomer solution obtained by fitting, it can be seen that there is a considerable difference between the two, especially the consistency coefficient K . This is because the calculated parameters are measured by a six-speed rotational viscometer and then calculated by Eqs. (4)–(6), while the parameters obtained by fitting are measured by an Anton Paar rheometer and then fitted to the relationship between shear rate and shear stress, so the parameters obtained by fitting are used.

$$\tau = 0.511\theta_3 \quad (4)$$

$$n = 3.322 \lg [(\theta_{600} - \theta_3)/(\theta_{300} - \theta_3)] \quad (5)$$

$$K = 0.511(\theta_{300} - \theta_3)/511^n \quad (6)$$

Experimental principles

The experiment was carried out by immersing spherical pellets into the solution with tweezers and releasing them at the center of the cylindrical tube. To reduce the influence of uncertainties such as human factors on the experiments, 3–5 experiments were carried out for each spherical particle in the same density solution to ensure at least 3 sets of valid experimental data. and in fitting the resistance coefficients, only experimental data with a relative error in velocity of less than 4% were selected.

It can be observed from the 167 sets of settling experiments that the regularly shaped round spherical particles settle very stably and freely along the center of the pipe, with almost no secondary motion. Therefore, it is considered that when the particles are subjected to a resistance force F_d (particle-liquid interaction force, Eq. (8)) equal to the difference between gravity F_g and buoyancy F_b (Eq. (9)), the sphere reaches an end velocity V_t [17–19].

$$F_d = F_g - F_b \quad (7)$$

which

$$F_d = \frac{\pi}{8} \rho_L C_D D_e^2 V^2 \quad (8)$$

Table 3 Comparison of rheological parameters of carbomer solutions

Fitted parameters			Calculated parameters		
τ_0 (Pa)	K (Pa.s ⁿ)	n	τ_0 (Pa)	K (Pa.s ⁿ)	n
0.289	0.0498	0.829	0.246	0.0228	0.843
0.254	0.0382	0.859	0.209	0.0177	0.872
0.231	0.0266	0.903	0.177	0.0125	0.914
0.206	0.0176	0.949	0.147	0.0084	0.958
0.192	0.0145	0.965	0.134	0.0070	0.973
0.110	0.0119	0.981	0.086	0.0057	0.989

$$F_g - F_b = \frac{\pi}{6}(\rho_s - \rho_L)gD_e^3 \quad (9)$$

where.

ρ_s : density of particles, kg/m³;

ρ_L : fluid density, kg/m³;

V : velocity difference between particles and fluid, m/s;

C_D : resistance coefficient, dimensionless.

The resistance coefficient C_D is crucial in characterizing the settling properties of particles. Since its formula includes the particle settling velocity V_t , The relative displacement (Δs) of particles between two frames (Δt) needs to be measured using the software "GetData" before calculating the C_D . The software GetData obtains the coordinates of a point on the picture by establishing the axes and unit lengths, which can be used to determine the positional coordinates of the particles at the time of settlement, and thus to obtain the relative displacements. and the settling velocity of the particles ($V_t = \Delta s / \Delta t$) is calculated. The expression for the resistance coefficient C_D is given in Eq. (10):

$$C_D = \frac{4}{3} \frac{\rho_s - \rho_L}{\rho_L} \frac{gD_e}{V_t^2} \quad (10)$$

The Reynolds number, Re_s , is another dimensionless number that must be determined to characterize the settling of particles. The significance of the Reynolds number is the ratio of the inertial force to the viscous force, which is used to determine whether the fluid flow is laminar ($Re_s \leq 2320$) or turbulent ($Re_s > 2320$), as well as the intensity of turbulence [20]. For the Herschel-Bulkley fluid, the formula is shown in Eq. (11):

$$Re_{s-HB} = \frac{\rho_L V_t^{2-n} D_e^n}{K + \tau_0 \left(\frac{D_e}{V_t}\right)^n} \quad (11)$$

where.

τ_0 : yield point of the fluid, Pa;

K : the consistency coefficient of the fluid, Pa.sⁿ;

n : the rheological index of the fluid, dimensionless.

Experimental steps and flowchart

Experimental step

1. Before conducting the experiment, the carbomer solution was introduced into the organic glass tube and allowed to stand for 12 h to ensure that the bubbles were fully released.
2. The pellet was immersed in carbomer solution using forceps and gently placed in the center of the round tube to allow it to settle freely.
3. A high-speed camera was used to record the movement of particles in a Plexiglas tube.
4. Each spherical particle experiment was conducted three times to reduce the interference of uncertain factors and improve the accuracy of experimental measurement results. When the debris particles settled, the experimental data whose trajectories deviated significantly from the center line of the circular tube were discarded.

Experimental flow chart

Figure 4 is a flow chart showing all the processes involved in the experimental study and modeling work on the sedimentation of dry heat rock cuttings.

Spherical particle settlement experiment and result analysis

Figure 5 shows the relationship between the experimentally measured C_D and Reynolds number Re_s plotted in logarithmic coordinates for the settlement resistance coefficient of the spherical particles. The classical Stokes formulation is obtained by Stokes by solving the Navier–Stokes equation by neglecting the nonlinear term in the laminar region to obtain a formula for the fluid drag force on a circular sphere in a viscous fluid moving at a slower speed (particle Reynolds number $Re_s < 0.1$). From Fig. 5, it can be seen that when $Re_s < 1$, the difference between the experimentally measured value of the resistance coefficient C_D , and the C_D -Stokes calculated by the Stokes equation is large, and through the processing of the experimental data, it can be obtained that the average relative error of the two has been as high as 17.55%. From Eq. 8, it can be seen that the Reynolds number is negatively correlated with the yield point and the consistency coefficient, so the difference will only increase with the dilution of the solution. There is a large error in predicting the settling resistance coefficient of spherical particles in Herschel-Bulkley fluid using the Stokes equation and the calculation gives an average error of up to 53.04%. This suggests that using the C_D - Re_s relation applicable to Newtonian fluids to calculate the coefficient of resistance for settling spherical particles in non-Newtonian fluids can produce large errors.

A variety of models for predicting resistance coefficients have been developed by previous authors, these models include distinguishing between Newtonian fluids and non-Newtonian fluids, as well as between regular particles and irregular particles. There are also differences in applicable types, Reynolds number ranges, model forms, etc. Some

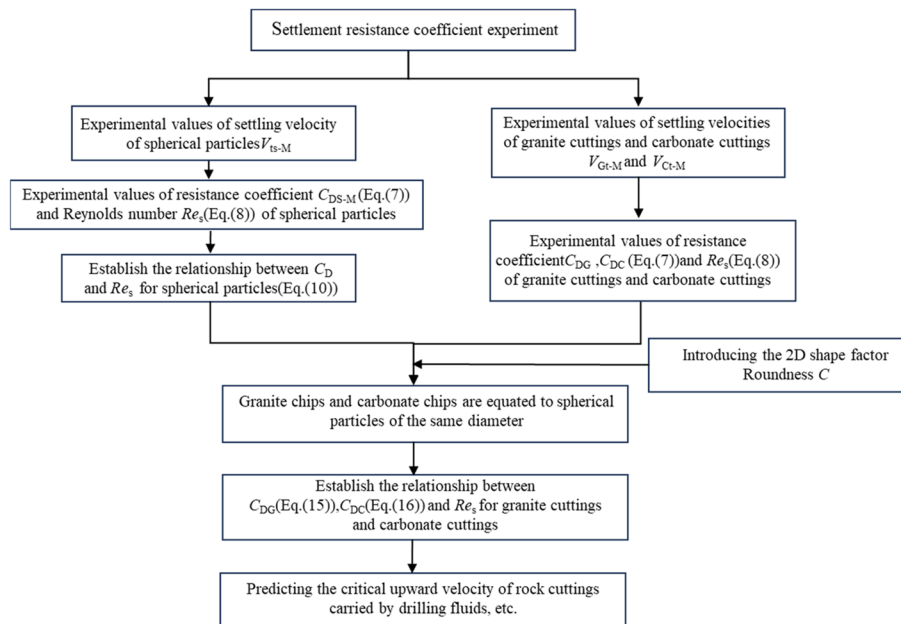


Fig. 4 Flow chart of settlement experiment of hot dry rock cuttings

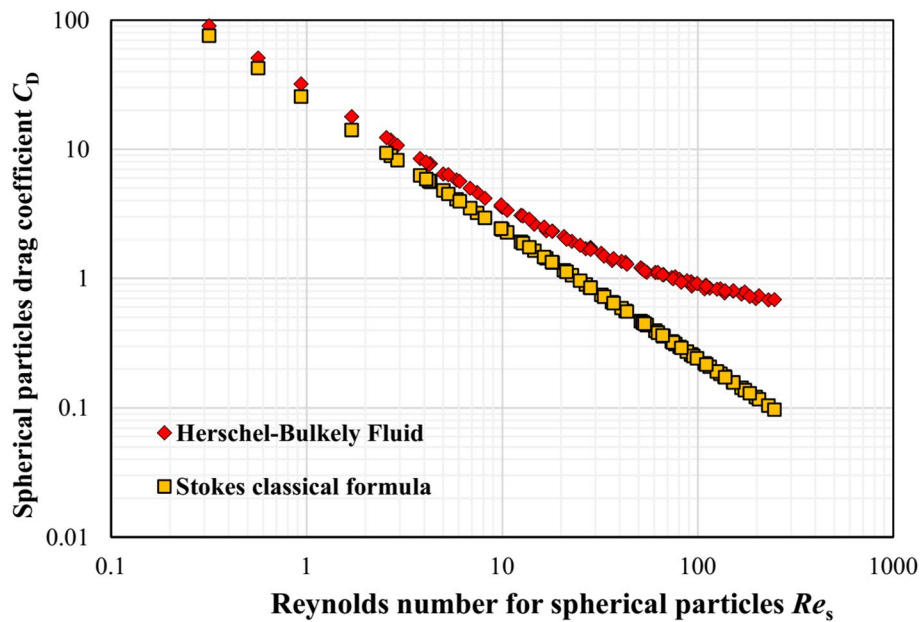


Fig. 5 C_D - Re_s relationship obtained from 167 groups of ball settlement experiments

of the more classical ones are Flemmer, Brown, Cheng, and Terfous [21–24]. Based on the experimentally obtained settlement data of 167 sets of round spherical particles, the above prediction model of settlement resistance coefficient was fitted, and it was found that the model proposed by Brown fitted best, As shown in Eq. (12).

$$C_D = \frac{24}{Re_s} (1 + ARe_s^B) + \frac{C}{1 + D/Re_s^E} \quad Re_s < 10^5 \tag{12}$$

where.

A, B, C, D, E : coefficients to be found, dimensionless.

The five unknown coefficients of Eq. 9 can be derived from the fitting, which leads to the C_D - Re_s relationship for the round spherical particles in the Herschel-Bulkley fluid as shown in Eq..

$$C_{DS} = \frac{24}{Re_s} (1 + 0.2151Re_s^{0.1361}) + \frac{0.5582}{1 + 0.0494/Re_s^{0.4862}} \quad 0.3 < Re_s < 247 \tag{13}$$

Equation (13) can demonstrate that the resistance coefficient C_D will decrease with the increase of Reynolds number in both the first and second terms of the right equation, which shows a negative correlation.

The experimentally obtained settlement resistance coefficients, the resistance coefficients calculated by Eq. (10), and the resistance coefficients obtained from previous studies are plotted in Fig. 6, which shows that the individual curves have the same trend. Among them, Khan [25], Okesanya [26], and the present experimental model are the C_D - Re_s relation obtained for the settling of round spherical particles in Herschel-Bulkley fluid. Therefore, to better reflect the accuracy of this experimental model, three error analysis parameters are used: root mean square error (*RMSE*), mean relative error (*MRE*), and coefficient of

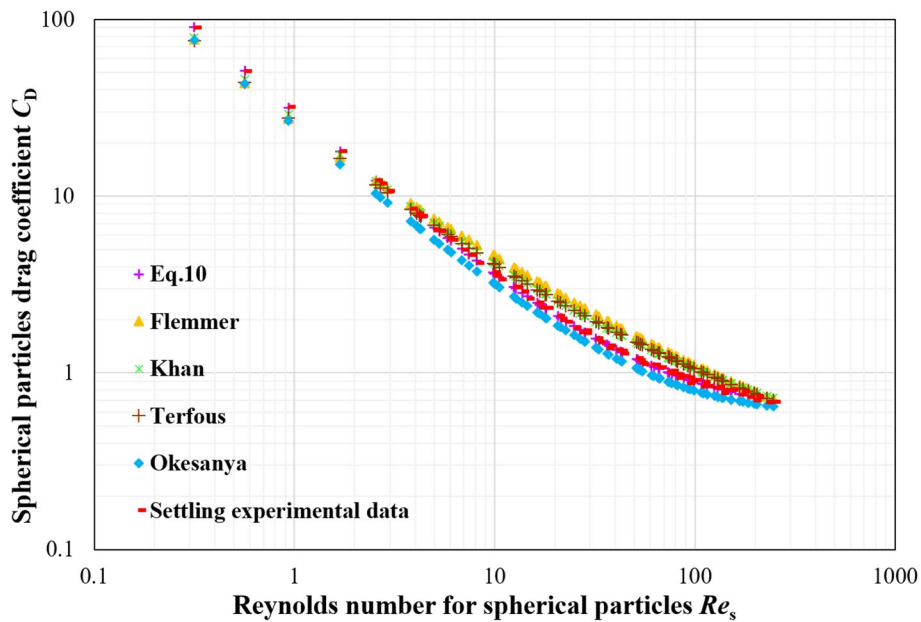


Fig. 6 Relationship between experimental and predicted C_D-Re_s of spherical particles

determination (R^2) [27, 28], The results are shown in Table 4. $RMSE$, MRE , and R^2 are shown in Eqs. (14)–(16).

$$RMSE = \sqrt{\frac{\sum_{i=1}^N (C_{DP} - C_{TM})^2}{N}} \tag{14}$$

$$MRE = \frac{\sum_{i=1}^N \frac{|C_{DP} - C_{DM}|}{C_{DM}}}{N} \times 100\% \tag{15}$$

$$R^2 = 1 - \frac{\sum_{i=1}^N (C_{DM} - C_{DP})^2}{\sum_{i=1}^N (C_{DM} - \overline{C_{DM}})^2} \tag{16}$$

Table 4 Error statistics of ball settlement resistance coefficient in Herschel-Bulkley fluid

Reynolds number range	Author	Errors		
		RMSE	MRE	R^2
0.3 < Re_s < 247	Khan (1987)	0.087	15.04%	0.992
	Okesanya (2020)	0.130	12.55%	0.987
	C_D-Re_s model of the paper (Eq. 13)	0.045	6.02%	0.998

where.

N : total number of experiment data points;

C_{DM} : experimental values of settlement resistance coefficient, dimensionless;

C_{DP} : predicted values of settlement resistance coefficient, dimensionless;

$\overline{C_{DM}}$: average experimental values of settlement resistance coefficients, dimensionless.

Resistance coefficient C_D , Reynolds number Re_s , and settling velocity V_t are nested with each other, so based on Eq. (13) in this paper, the iterative method can be used to calculate new predicted values of settling velocity and resistance coefficient, and compare the predicted values with the experimental values of settling velocity and resistance coefficient, and the iterative flowchart is shown in Fig. 7, and the results of the comparison are shown in Fig. 8.

From the results of the error analysis in Table 4, it can be seen that the *RMSE* and R^2 of the predicted values of Okesanya's model have the largest difference from the experimental measurements, and the *MRE* of the predicted values of Khan's model has the largest difference of 15.04% from the experimental measurements. The *RMSE* and *MRE* of the predicted values of the model in this paper are 0.045 and 6.02% respectively there is a substantial reduction and the coefficient of determination R^2 is 0.998 is the highest compared to other models. Therefore, the model proposed in this paper can better predict the settling resistance coefficient C_D , and settling velocity V_t , for spherical particles in Herschel-Bulkley fluids.

Settlement experiment of irregularly shaped hot dry rock cuttings

The lift and resistance forces on irregularly shaped dry heat cuttings during settling are related to some factors such as the shape of the particles and the direction of the force. This will result in higher resistances on the dry heat rock cuttings than on the spherical particles in the same solution [29]. Therefore, using Eq. to calculate the settlement resistance coefficient of dry heat rock cuttings will result in inaccurate calculations of parameters such as the height of the bed of cuttings and the volume of discharge needed to carry the rock, which leads to engineering problems such as plug-hole jamming, well-wall collapses, etc. In addition, irregular cuttings may drift when settling, failing to fall steadily along the center of the pipe or even spiraling downwards, a phenomenon that is evident in the settling of flake granite cuttings. As shown in Fig. 9, particles of similar mass but different shapes in the settlement experiments were selected, as shown in the figure, when the particles were close to falling at a uniform velocity, the regularly shaped aluminum spheres had the fastest settling velocity of about 0.28 m/s because they were subjected to the least resistance, whereas the highly irregularly shaped flakey granite cuttings had the slowest settling velocity of about 0.06 m/s because they were subjected to the greatest resistance. Therefore, to avoid the influence of wall effects and secondary motions, the settlement resistance coefficients of all cuttings that adhere to the wall (near the wall), flip, or spiral sink are deleted when processing the experimental data. and introduce a form factor- Roundness to modify Eq. (13).

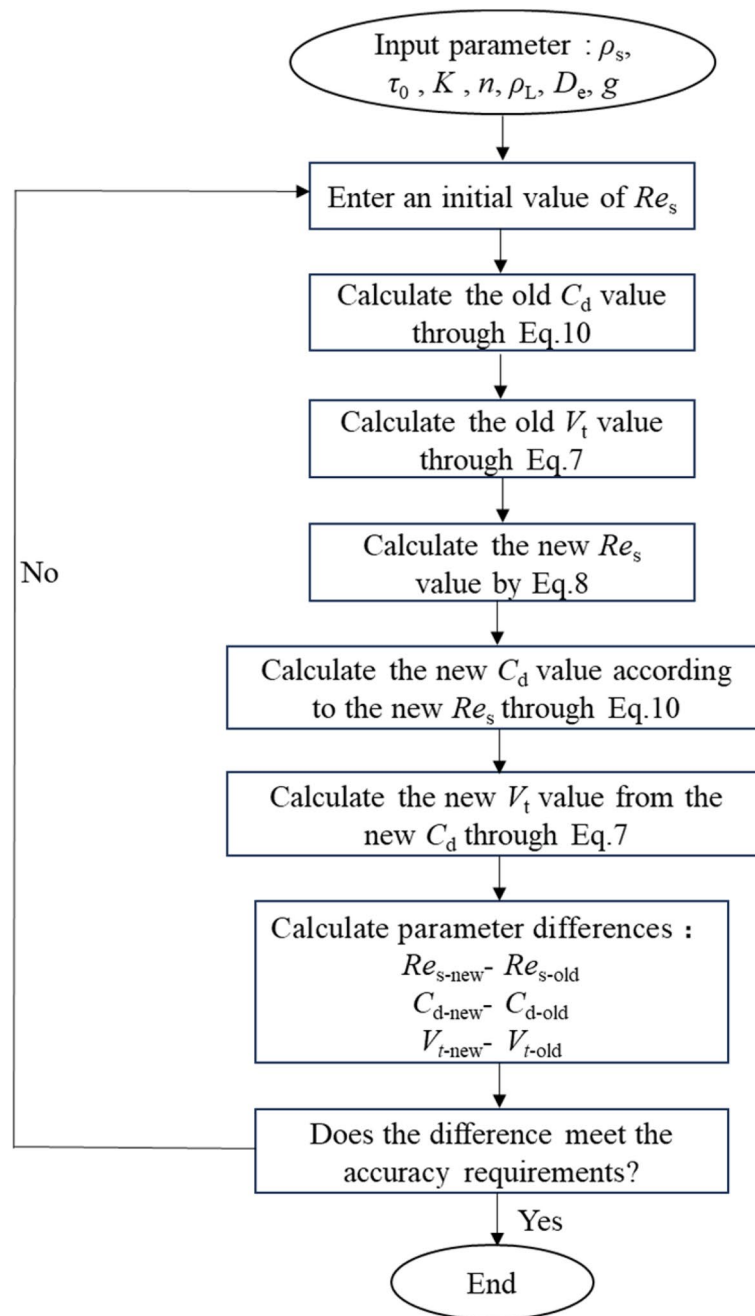


Fig. 7 Schematic diagram of parameter iteration

The ratios of the experimental values of settlement resistance coefficients C_D and their equivalent spherical settlement resistance coefficients predicted values C_{DS} were calculated for 153 granite cuttings and 174 carbonate cuttings respectively, and the results were plotted as shown in Fig. 10. It can be seen that the C_D/C_{DS} of both cuttings is slightly greater than 1. Based on the analysis of experimental data, to better reflect the relationship between roundness and Reynolds number and to ensure that the particles are spherical (when the roundness is 1) to meet the $C_D/C_{DS} = 1$, This paper uses Eq. (17) to calculate the settlement resistance coefficient of cuttings.

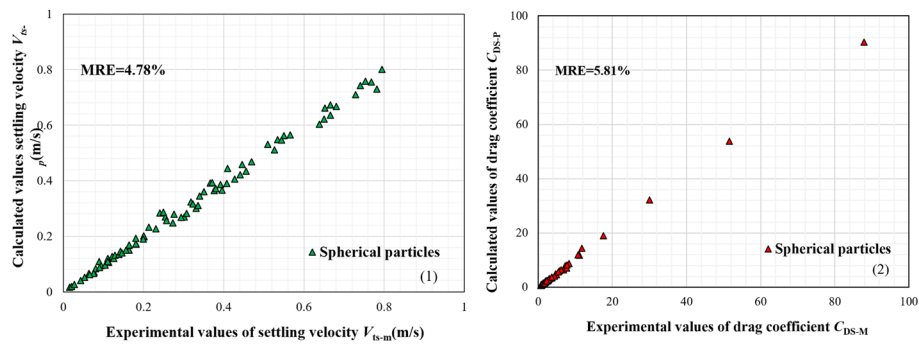


Fig. 8 Comparison of predicted and experimental values of spherical settlement: 1 settlement velocity; 2 resistance coefficient

$$C_D = C_{DS} \exp \left[X Re_s^Y (1 - c)^Z \right] \tag{17}$$

where.

X, Y, Z : coefficient to be found, dimensionless.

Substituting the results of the data fitting and Eq. into Eq., the expressions for the coefficient of resistance coefficient of settlement C_D for granite cuttings and carbonatite cuttings in Herschel-Bulkley fluid are obtained as shown in Eqs. (18) and (19).

Granite cuttings:

$$C_{DG} = \left(\frac{24}{Re_s} (1 + 0.2151 Re_s^{0.1361}) + \frac{0.5582}{1 + 0.0494 / Re_s^{0.4862}} \right) \exp \left[1.131 Re_s^{-0.004} (1 - c)^{-0.036} \right] \tag{18}$$

Carbonate cuttings:

$$C_{DC} = \left(\frac{24}{Re_s} (1 + 0.2151 Re_s^{0.1361}) + \frac{0.5582}{1 + 0.0494 / Re_s^{0.4862}} \right) \exp \left[1.16 Re_s^{-0.006} (1 - c)^{0.035} \right] \tag{19}$$

Results and discussion

Figure 11 shows the comparison between the predicted and experimental values of resistance coefficients for granite cuttings and carbonate cuttings, respectively. Table 5 presents the results of the error evaluation for the two prediction models. It can be seen that the predicted values $RMSE$ and MRE calculated by Eq. (19) are lower, 0.027 and 6.59% respectively, while the predicted value R^2 calculated by Eq. (18) is higher at 0.980.

Based on the C_{DG} and C_{DC} models, iterative calculations were used to obtain the predicted values of settling velocities V_{Gt-P} and V_{Ct-P} for granite cuttings and carbonatite cuttings in Herschel-Bulkley fluids, which were compared with the experimental values V_{Gt-M} and V_{Ct-M} , respectively, and the results are shown in Fig. 12. The average relative errors between the predicted and experimental values of the settling velocities of the two dry heat rock chips are 7.27% and 6.21%. Therefore, the V_{Gt} model and V_{Ct} model can better predict the settling velocity of two types of dry hot rock cuttings in the Herschel-Bulkley fluid.

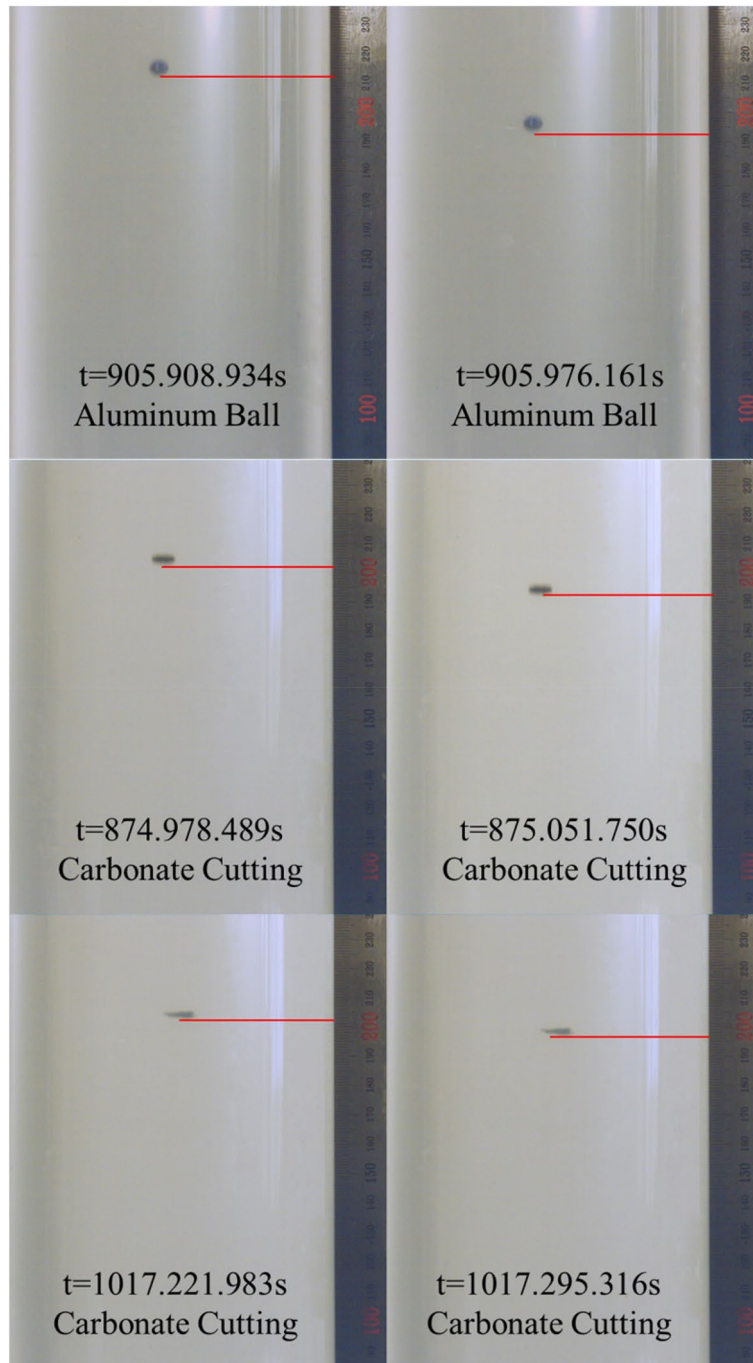


Fig. 9 Settlement diagrams for particles of different shapes

Conclusions

To study the settlement characteristics of particles in Herschel-Bulkley fluid, a total of 494 sets of valid settlement experimental data were selected (167 sets of spheres, 153 sets of granite cuttings, and 174 sets of carbonate cuttings). Through the analysis of the above experimental data, the following conclusions are drawn:

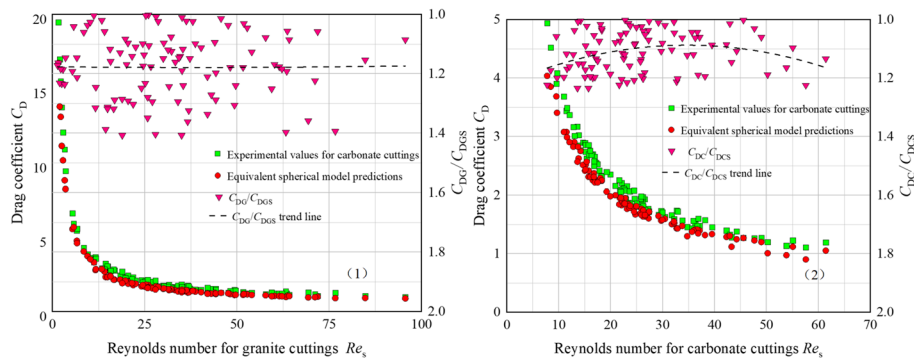


Fig. 10 C_D - Re_s relationship diagram obtained from the experiment: 1 153 groups of granite cuttings, 2 174 groups of carbonate cuttings

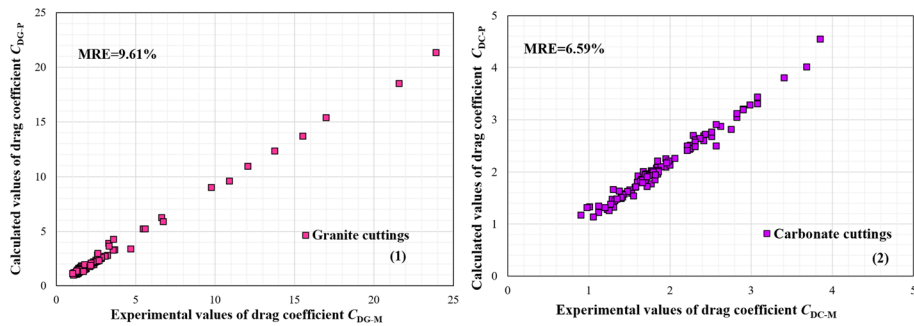


Fig. 11 Comparison of experimental values and prediction values of cutting resistance coefficient: 1 granite cuttings, 2 carbonate cuttings

Table 5 Error statistics of two types of debris settlement resistance coefficients

Type of cuttings	Range of Reynolds numbers	Errors		
		RMSE	MRE	R^2
Granite cuttings	$1.42 < Re_s < 99$	0.063	9.61%	0.980
Carbonate cuttings	$7.76 < Re_s < 61$	0.027	6.59%	0.962

- (1) Based on the model proposed by Brown, this paper considers the influence of the rheology of Herschel-Bulkley fluid on the resistance coefficient, corrects the correlation coefficient, and constructs a prediction model C_{DS} based on Herschel-Bulkley fluid that is consistent with the settlement resistance coefficient of spherical particles. The *MRE* between the predicted value C_{DS-P} and the experimental value C_{DS-M} is 6.02%.
- (2) Characterization of highly irregular granite cuttings and carbonate cuttings using Roundness based on C_{DS} modeling, The resistance coefficient prediction models C_{DG} for granite cuttings and C_{DC} for carbonate cuttings in Herschel-Bulkley fluids were constructed, respectively. The *MRE* between the predicted and experimental values of resistance coefficients for the two types of cuttings were 9.61% and 6.59%, respectively.

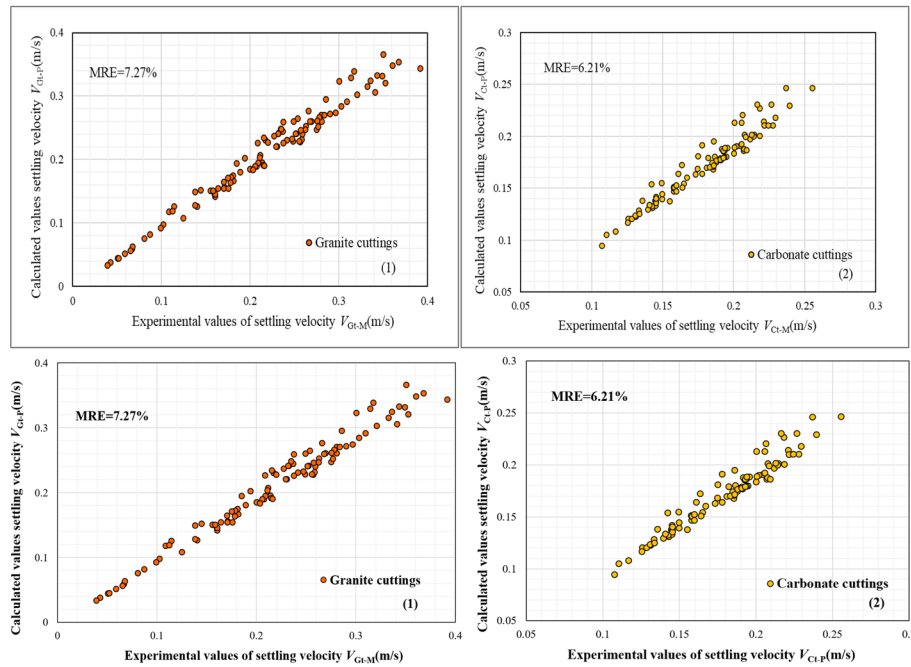


Fig. 12 Comparison of experimental values and prediction values of cuttings settling velocity: 1 granite cuttings, 2 carbonate cuttings

- (3) Based on the C_{DG} model and C_{DC} model, the iterative method is used to reversely calculate the settlement velocity. The MRE between the predicted and experimental values of settlement velocity for granite rock chips and carbonate rock chips can be obtained as 7.27% and 6.21%, respectively. Once again, both the C_{DG} and C_{DC} models are confirmed to have good predicted effects. This lays the foundation for subsequent more accurate calculations of cutting bed height, drag force, and other parameters, as well as more accurate modeling for predicting the restart of cuttings. It can provide a theoretical basis and engineering application guidance for solving borehole cleaning problems and optimizing hydraulic parameters in the drilling construction of geothermal wells in dry hot rocks.
- (4) One of the limitations of this article is that the test solution used is not a real drilling fluid because drilling fluids are usually formulated with a large amount of materials such as bentonite. However, the use of bentonite cannot guarantee the visibility of the experiment and cannot observe the movement of particles in the solution. Condition. The second limitation is that the Reynolds number range of the granite cuttings resistance coefficient model established in this article is 1.42–99, and the Reynolds number range of the carbonate cuttings resistance coefficient model is 7.7642–61. Within this range, the prediction accuracy of the resistance coefficient model established in this article is better than that of previous researchers. However, the range of Reynolds numbers should be expanded in future research so that the model in this article has a wider application range [18, 19, 23, 24].

Abbreviations

C_D	Resistance coefficient, dimensionless
C_{DS}	Calculated equivalent spherical settlement resistance coefficients for cuttings, dimensionless
C_{DM}	Experimental values of settlement resistance coefficient, dimensionless
C_{DP}	Calculated values of settlement resistance coefficient, dimensionless
C_{DS-M}	Experimental value of resistance coefficient of spherical particles, dimensionless
C_{DS-P}	Calculated value of resistance coefficient of spherical particles, dimensionless
C_{DG-M}	Experimental value of resistance coefficient of granite cuttings, dimensionless
C_{DG-P}	Calculated value of resistance coefficient of granite cuttings, dimensionless
C_{DC-M}	Experimental value of resistance coefficient of carbonate cuttings, dimensionless
C_{DC-P}	Calculated value of resistance coefficient of carbonate cuttings, dimensionless
C_{DM}	Average experimental values of settlement resistance coefficients, dimensionless
D_e	Equivalent diameter, mm
D_{eg}	Equivalent diameter of granite cuttings, mm
D_{ec}	Equivalent diameter of carbonate cuttings, mm
F_d	Resistance force, N
F_g	Gravity, N
F_b	Buoyancy, N
K	Consistency coefficient of the fluid, $\text{Pa}\cdot\text{s}^n$
m_p	Quality of pellets, kg
MRE	Mean relative error
n	Rheological Index of the fluid, dimensionless
P_a	Perimeter of the equivalent sphere of the projected surface of the particle, m
P_b	The projected perimeter of the particle, m
$RMSE$	Root mean square error
R^2	Coefficient of determination
V	Velocity difference between particles and fluid, m/s
V_{TS-M}	Experimental values settling velocity of spherical particles, m/s
V_{TS-P}	Calculated values settling velocity of spherical particles, m/s
V_{GT-M}	Experimental values settling velocity of granite cuttings, m/s
V_{GT-P}	Calculated values settling velocity of granite cuttings, m/s
V_{CT-M}	Experimental values settling velocity of carbonate cuttings, m/s
V_{CT-P}	Calculated values settling velocity of carbonate cuttings, m/s
X	Roundness, dimensionless
τ	Shear stress, Pa
τ_0	Yield point, Pa
γ	Shear rate, $1/\text{s}$
ρ_s	Density of particles, kg/m^3
ρ_L	Density of fluid, kg/m^3
Re_s	The Reynolds Number, dimensionless
Re_{s-HB}	The Reynolds Number of Herschel-Bulkley Fluid, dimensionless

Acknowledgements

All authors are sincerely grateful to all organizations and individuals who have helped with this article.

Authors' contributions

The first author: Lei Wang performed the data analysis and wrote the manuscript. The second and correspondence author: Jinhui Li performed the experiments and participated in the manuscript writing. The third author: Jianjun Zhao made important contributions to the analysis and manuscript writing. The fourth author: Shulong Wang contributed to the study conception. The fifth author: Chu Zheng helped with the analysis and conducted constructive discussion. All authors have read and approved the final manuscript.

Funding

National Natural Science Foundation of China (Grant No. 52192624); National Key Research and Development Program of China (No. 2019YFC0604904, 2019YFB1504201).

Availability of data and materials

If you need to obtain specific experimental data, if privacy and confidentiality permit, please contact the corresponding author to provide it.

Declarations

Competing interests

All authors declare that they have no competing interests.

Received: 26 November 2023 Accepted: 25 April 2024

Published online: 06 May 2024

References

1. Lin WJ, Wang GL, Gan HN, Wang AD, Yue GF, Long XT (2022) Heat generation and accumulation for Hot Dry Rock resources in the igneous rock distribution areas of southeastern China. *Lithosphere* 2021(Special 5):2039112. <https://doi.org/10.2113/2022/2039112>
2. Yuan RX, Zhang W, Gan HN, Liu F, Wei SC, Liu LX (2022) Hydrochemical characteristics and the genetic mechanism of low–medium temperature geothermal water in the Northwestern Songliao Basin. *Water* 14(14):2235. <https://doi.org/10.3390/w14142235>
3. Jian O, Chen LJ, Zhang BJ, Zhou H, Tang XC, Bai HQ, Zhang DL, Gao J (2022) The formation mechanism of the typical hot dry rocks in Hunan Province China. *J Geophys Eng* 19(6):1246–1264. <https://doi.org/10.1093/jge/gxac080>
4. Gao WL, Zhao JT, Peng SP (2022) UNet–based temperature simulation of hot dry rock in the Gonghe Basin. *Energies* 15(17):6162. <https://doi.org/10.3390/en15176162>
5. He K, Huang R, Xu YX, Hu SQ, Wei PL (2022) Crustal structures beneath the Northern Jiangsu Basin and its surrounding areas: implications for geothermal prospecting. *J Geophys Eng* 19(3):316–325. <https://doi.org/10.1093/jge/gxac018>
6. Wang G, Dong MK, Wang ZF, Ren T, Xu SJ (2022) Removing cuttings from inclined and horizontal wells: Numerical analysis of the required drilling fluid rheology and flow rate. *J Nat Gas Sci Eng* 102:104544. <https://doi.org/10.1016/j.jngse.2022.104544>
7. Ahonguo F, Jossic L, Magnin A (2014) Influence of surface properties on the flow of a yield stress fluid around spheres. *J Nonnewton Fluid Mech* 206:57–70. <https://doi.org/10.1016/j.jnnfm.2014.03.002>
8. Elgaddafi R, Ahmed R, Growcock F (2016) Settling behavior of particles in fiber-containing herschel bulkley fluid. *Powder Technol* 301:782–793. <https://doi.org/10.1016/j.powtec.2016.07.006>
9. Hakim H, Katende A, Sagala F, Ismail I, Nsamba H (2018) Performance of polyethylene and polypropylene beads towards drill cuttings transportation in horizontal wellbore. *J Petrol Sci Eng* 165:962–969. <https://doi.org/10.1016/j.petrol.2018.01.075>
10. Katende A, Boyou NV, Ismail I, Chung DZ, Sagala F, Hussein N, Ismail MS (2019) Improving the performance of oil based mud and water based mud in a high temperature hole using nanosilica nanoparticles. *Colloids Surf, A* 577:645–673. <https://doi.org/10.1016/j.colsurfa.2019.05.088>
11. Heshamudin NS, Katende A, Rashid HA, Ismail I, Sagala F, Samsuri A (2019) Experimental investigation of the effect of drill pipe rotation on improving hole cleaning using water-based mud enriched with polypropylene beads in vertical and horizontal wellbores. *J Petrol Sci Eng* 179:1173–1185. <https://doi.org/10.1016/j.petrol.2019.04.086>
12. Yeu WJ, Katende A, Sagala F, Ismail I (2019) Improving hole cleaning using low density polyethylene beads at different mud circulation rates in different hole angles. *J Nat Gas Sci Eng* 61:333–343. <https://doi.org/10.1016/j.jngse.2018.11.012>
13. Zhao X, Qiu Z, Huang W, Wang M (2017) Mechanism and method for controlling low-temperature rheology of water-based drilling fluids in deepwater drilling. *J Petroleum Sci Eng* 154:405–416. <https://doi.org/10.1016/j.petrol.2017.04.036>
14. Majid NF, Katende A, Ismail I, Sagala F, Sharif NM, Che Yunus MA (2019) A comprehensive investigation on the performance of durian rind as a lost circulation material in water based drilling mud. *Petroleum* 5(3):285–294. <https://doi.org/10.1016/j.petlm.2018.10.004>
15. Wadell H (1932) Volume, shape, and roundness of rock particles. *J Geol* 40(5):443–451. <https://doi.org/10.1086/623964>
16. Naganawa S (2013) Experimental study of effective cuttings transport in drilling highly inclined geothermal wells. *J Jap Assoc Petroleum Technol* 78(3):257–264. <https://doi.org/10.3720/japt.78.257>
17. Fan M, Su D, Yang L (2022) Development of a benchmark for drag correlations of nonspherical particles based on settling experiments of super-ellipsoidal particles. *Powder Technol* 409:117811. <https://doi.org/10.1016/j.powtec.2022.117811>
18. Katende A, Segar B, Ismail I, Sagala F, Saadiah HHAR, Samsuri A (2020) The effect of drill–pipe rotation on improving hole cleaning using polypropylene beads in water-based mud at different hole angles. *J Petroleum Explor Prod Technol* 10:1253–1262. <https://doi.org/10.1007/s13202-019-00815-1>
19. Choi CE, Zhang JQ, Liang ZY (2022) Towards realistic predictions of microplastic fiber transport in aquatic environments: Secondary motions. *Water Res* 218:118476. <https://doi.org/10.1016/j.watres.2022.118476>
20. Sofiadis G, Sarris I (2022) Reynolds number effect of the turbulent micropolar channel flow. *Physics of Fluids* 34(7). <https://doi.org/10.1063/5.0098453>
21. Flemmer RL, Banks CL (1986) On the drag coefficient of a sphere. *Powder Technol* 48(3):217–221. [https://doi.org/10.1016/0032-5910\(86\)80044-4](https://doi.org/10.1016/0032-5910(86)80044-4)
22. Terfous A, Hazzab A, Ghenaim A (2013) Predicting the drag coefficient and settling velocity of spherical particles. *Powder Technol* 239:12–20. <https://doi.org/10.1016/j.powtec.2013.01.052>
23. Brown PP, Lawler DF (2003) Sphere drag and settling velocity revisited. *J Environ Eng* 129(3):222–231. [https://doi.org/10.1061/\(ASCE\)0733-9372\(2003\)129:3\(222\)](https://doi.org/10.1061/(ASCE)0733-9372(2003)129:3(222))
24. Cheng NS (2009) Comparison of formulas for drag coefficient and settling velocity of spherical particles. *Powder Technol* 189(3):395–398. <https://doi.org/10.1016/j.powtec.2008.07.006>
25. Khan AR, Richardson JF (1987) The resistance to motion of a solid sphere in a fluid. *Chem Eng Commun* 62(1–6):135–150. <https://doi.org/10.1080/00986448708912056>
26. Okesanya T, Kuru E, Sun YX (2020) A new generalized model for predicting the drag coefficient and the settling velocity of rigid spheres in viscoplastic fluids. *SPE J* 25(06):3217–3235. <https://doi.org/10.2118/196104-PA>
27. Rushd S, Hassan I, Sultan RA, Kelessidis VC, Rahman A, Hasan HS, Hasan A (2018) Terminal settling velocity of a single sphere in drilling fluid. *Part Sci Technol*. <https://doi.org/10.1080/02726351.2018.1472162>
28. Yang F, Zeng YH, Huai WX (2021) A new model for settling velocity of non-spherical particles. *Environ Sci Pollut Res* 28:61636–61646. <https://doi.org/10.1007/s11356-021-14880-9>
29. Chen S, Chen PZ, Fu JH (2022) Drag and lift forces acting on linear and irregular agglomerates formed by spherical particles. *Physics of Fluids* 34(2). <https://doi.org/10.1063/5.0082653>